Stresses in the Vicinity of an Un-reinforced Mitre Intersection: An Experimental and Finite Element Comparison

J. Wood[a]

[a] Department of Mechanical Engineering, University of Strathclyde, 75 Montrose Street, Glasgow G1 1XJ, UK

Abstract

The experimental investigation reported, provides elastic stresses in the vicinity of the un-reinforced intersection of a single 90º mitred bend, subjected to an in-plane bending moment. The specimen was extensively strain gauged on the outer surface. A small number of rosettes were also laid on the inside surface close to the welded intersection. The procedures used for the successful installation of the inside surface gauges are discussed. In the experiment, consideration was also given to deflections and rotations. Satisfactory comparisons with adaptive-p thin shell finite element results were obtained in general and differences are explained in terms of the known experimental variables and finite element approximations. The nature of the stresses at such intersections is discussed and various methods of obtaining fatigue 'hot-spot' stresses are considered.

Keywords: Single Unreinforced Mitred Bend; Elastic; Experimental; Finite Element Analysis; Hot-spot Stress

Article Outline

1. Introduction

The experimental investigation reported herein, provides elastic stresses for a single un-reinforced 90º mitred bend, subjected to an in-plane bending moment. Like smooth bends, mitred bends result in an increase in flexibility, as well as an increase in local stress levels. These effects are due to cross section ovalisation under load. Unlike a smooth bend however, the stress distribution in a mitred bend is further complicated due to the mitre discontinuity.

The strain gauge installation, shown in figure 1, provides comprehensive experimental data, for the mitred bend. The detailed results in the vicinity of the intersection provide a useful basis for comparison with thin shell finite element results, as well as providing the basis for comment on the various techniques available for the retrieval of fatigue hot-spot stresses.

Effective fatigue assessment requires the determination of sufficiently accurate stresses to compare with available fatigue test data and allowables. The stress used in such an assessment will be a function of the type of detail being assessed and the particular Code of Practice or guidelines being used.

It has long been recognised that the detailed stress state at the discontinuous intersection of shell structures cannot be described completely by simple shell theory, in which the geometry of the structure is defined by wall centrelines or mid-surfaces and wall thicknesses. As a result, various techniques have been developed over the years in an attempt to improve the stresses obtained in thin shell models **[1]**. These developments include methodologies to represent any welds that may be present **[2]**. In the present case, the weld has been ground in an attempt to produce an 'ideal' mitre profile and therefore no use has been made of such techniques.

Three-dimensional elastic stress analysis at a re-entrant corner (such as the toe of a weld or mitre intersection) results in a theoretically infinite stress. Fatigue assessment procedures are not based on the direct use of stresses from finite element meshes at such locations because, with no fillet radius to blunt the stress level, any solid representation of such geometry will produce a stress level at the corner that converges to infinity with mesh refinement. The ***finite*** value of stress provided by any particular ***finite*** element mesh is therefore non-converged and is a function of mesh refinement. Shell representation of the mitre does not suffer from this type of singularity at the intersection, although singularities can exist with shell models in general. It is however commonly observed that calculated thin shell stresses at such an intersection are often too high – particularly when the effects of any welds have not been included in the models. In such circumstances, stresses are often extrapolated to the weld toe location. As an alternative, reference **[3]** notes that extrapolation to the intersection should be considered to avoid under-estimation at the weld-toe location. However, as will be shown in the present study, not all components of stress are maximum at the intersection. Care should therefore be taken in selecting appropriate thin shell locations for assessment purposes.

Various extrapolation procedures have been developed to obtain repeatable and converged nominal values of stress at these locations, as illustrated in figure 2. The extrapolation procedures are also used to remove any singularity stresses present in solid representations and also to remove the local peak stresses due to the particular

weld geometry. The reason for this is that fatigue allowables often already include such local effects **[3, 4, 5]**. These stresses are referred to as 'hot-spot' stresses or 'structural' stresses. Clearly these stresses are representative in nature and will not necessarily exist at any point in the model or the real structure.

Such extrapolation procedures have been used for many years. In the late 1970s and early 80's much work in this area was being carried out as part of the United Kingdom Offshore Steels Research project **[6]** in the study of stresses in the joints of tubular jacket structures. In this case both experimental strain gauging and finite elements were being used as a means of determining the toe hot-spot stresses. Comparisons with photoelastic models were also made. Indeed the guidelines in reference **[3]** provide different extrapolation methods for use with strain gauges and finite element modelling. The latter also includes different guidance for 'coarse' and 'fine' meshes. Fine mesh quadratic extrapolation (3 points) is recommended in special cases where it is not possible to use the guidelines e.g. due to the closeness of two welds. The guidelines also introduce the notion of type 'a' and 'b' hot-spots, with different procedures for handling both. Interestingly the guidance on meshing accepts that non-converged results (coarse meshes) may be used as long as there are no other severe discontinuities in the vicinity; that the stress gradient is not high; that standard 8-noded shell elements or 20-noded solids are used and that the stresses used are those at the mid-side nodes. It is argued that the error introduced by using relatively distant extrapolation points is compensated by the slightly exaggerated midside node stresses due to the influence of the singularity at the hot-spot corner node. Such guidance is clearly arising from the practicalities of modelling large fabricated structures, where representation of detail as small as welds is not practical. However, it is apparent that converged results would provide a more consistent and logical basis for any extrapolation method. Ideally, extrapolation methods should not be a function of the shape function of elements used or the degree of mesh refinement. No doubt such guidance will evolve, as available computing resources continue to increase. The converged results from the highly refined model of the mitre can possibly be used as the basis for studying such developments and this is discussed further in section 4.3.

2. Experiment

2.1. Test Rig

The test rig utilized a simple 'goal-post' arrangement to subject the bend to a transverse load via a hydraulic ram, as shown in figure 3. This method of loading subjected the horizontal leg of the bend to a linearly varying bending moment, in addition to a shearing action. The vertical leg, on the other hand, was subjected to a uniform bending moment in addition to a thrust action.

In the experimental set-up shown in figure 3, the effect of the self-weight of the horizontal leg was removed by use of a pulley arrangement.

This general test configuration and data was also used as the basis for the finite element model, as shown in figure 4.

2.2. Bend Specification and Manufacture

The test specimen shown in figure 3 was manufactured from carbon steel hot finished seamless pipe **[7]**, with nominal dimensions of 200mm dia.x 6.35mm thk. The measured bend angle of 89.2º resulted from inaccurate 'fit-up' during the welding of the mitre. The intersection weld was ground flat.
A thickness survey was carried out on the bend with an ultrasonic digital thickness meter and values were measured at 79 locations on each leg. The average thickness was 6.53mm with a variation of ±4.5%. A diameter survey across 28 diameters on each leg was also carried out, before and after welding. The average OD was 193.9mm with a variation of ±0.7%. These values are well within the tolerances permitted by reference **[7]**. The thickness variation can have a significant effect on the experimental stress values and this is discussed in section 4. It clearly would have been possible to use pipe with a higher degree of tolerance on geometry. However, the purpose of this paper was not to report a highly accurate comparison between finite element analysis and experiment, but to illustrate the real variations and practical challenges that comparisons between idealized finite element models and 'as-built' structures entails.

A total of eight tensile test specimens were manufactured from the pipe and tested in accordance with BS EN 10002-1 **[8]**. Two of the specimens had strain gauge 'pairs' attached, to facilitate the determination of Poisson's ratio. The average values of 'E = 209 kN/mm^2' and '$\nu = 0.28$' were used in the finite element analyses.

2.3. Instrumentation and Ancillary Equipment

Details of the electrical resistance strain gauges and the installation used in the experiment are shown in table 1. All strain gauges were installed in accordance with the guidelines given in references **[9, 10]**, with respect to surface preparation and bonding. After installation, checks were made on 'resistance-to-earth' and 'gauge resistance', for all strain gauges. Gauges operated satisfactorily throughout the test. A total of 46 'rosettes' and 4 'pairs' were attached to the bend and these were connected into the data logger in a 4-wire ¼ bridge configuration.

To install the inside surface gauges, the horizontal leg of the bend was cut approximately 200mm from the intersection, as indicated by the position of the weld in figure 1. The actual length of pipe left had to be short enough to allow strain gauge installation close to the mitre, but not too short so as to avoid damage to the gauges during the re-welding of the leg. The inner surface gauges were covered with fire protection cloth during re-welding, to prevent weld 'spatter' damage. During the re-welding operation, the region of the intersection was continually cooled by a water jacket and the temperature in the region of the gauges monitored with 'temperature indication sticks'.

All gauges in the vicinity of the mitre intersection were in the form of rosettes, to enable the principal stresses and their directions to be determined. The inner and outer surface 'hoop' distributions of gauges were located as close to the mitre intersection as the gauge backing would allow. The smallest rosettes had individual gauge lengths of 0.38mm, to enable the steep stress gradients to be accurately measured.

The 90º and 60º positions were chosen for the 'longitudinal' distributions of gauges. The 60º position is in the region of maximum stress, as shown in the finite element

results. In addition, the 90º location possesses the characteristic of not having any slope discontinuity between the shells.

Strain gauge 'pairs' located one metre from the intersection, allowed an assessment of loading symmetry to be made, in addition to providing a 'membrane' check. The rosettes at the -90º and -60º positions on the outer surface at the intersection, also provided a check on loading symmetry.

All gauges used in the experiment were temperature compensated for steel. The energization current for all gauges was 8.3mA. The gauges were scanned and energized at the rate of 40 per second and no difficulty was experienced due to self-heating of the gauges.

The transverse load was applied to the bend by an 'Enerpac' hydraulic ram of 30 kN capacity, as shown in figure 3. A 'needle' valve was included in the hydraulic circuit to permit accurate control of the loading. The loading arrangement consisted of the hydraulic ram, a load cell, a ball bearing resting in a spherical seat to take up any misalignment of loading and also a bearing pad to distribute the load to the bend. The calibrated load cell used in the experiment provided a good strain output for the load levels applied.

Dial gauges with a resolution of 0.01 mm were used to measure both the bend and rig deflection. The latter was found to be negligible. The dial gauges were located on a frame built up from the floor. End rotation of the bend was measured by a laser beam, which was deflected by a mirror attached to the end of the horizontal leg of the pipe onto a measurement chart.

2.4. Experimental Procedure

Some relevant details of the experimental procedure are outlined below:
(i) The maximum load to be applied was established by monitoring all gauges at a low load level. The strain gauge exhibiting the highest strain level was established and this value of strain was used to determine the load that would result in a strain of 1000 με for this particular gauge.
(ii) The load was cycled 5 times from zero to maximum value.
(iii) During the test, checks were made on the symmetry of loading and adjustments were made to the ram position as necessary.
(iv) Loads were applied in 10, approximately equal, increments up to the maximum. The loading was decreased from the maximum in 5, approximately equal, increments down to zero. Dial gauge, laser and strain gauge readings were taken at each increment and all readings were linear with applied load.

The experimental stress results were processed using strain gauge analysis software. The program analysed the various gauge configurations and also checked gauge linearity. For loading and unloading, the maximum deviation from the 'combined' best-fit straight line was insignificant.

3. Finite Element Model

Over the years numerous finite element analyses of mitred bends have been carried out, invariably using thin shell idealisations. Sobieszczanski **[11]** recommended such an approach over 35 years ago for this problem. Possibly the earliest reference to the actual use of finite elements, for the study of a mitred bend, is due to Edwards **[12]** in 1974. A comprehensive review of mitred bend publications from 1952 to date, is presented in reference **[13]**. This review contains reference to 93 publications, many of which detail the development of analytical solutions by Kitching and others. However, given the stated purpose of the present investigation, comparisons with such analytical results are not presented.

The finite element model of the experimental specimen used in the present investigation is shown in figure 4. The end of the vertical leg was assumed fully fixed. A half model was used as a result of symmetry. The finite element results presented were produced using shell elements, as implemented in the Pro-Mechanica Applied Structure system from Parametric Technology Inc. The Applied Structure system uses adaptive-p element technology, which allows the user to specify a percentage convergence for the analysis. In the analyses reported here, convergence was based upon displacements, strain energy and a global root-mean-squared stress measure. Convergence levels achieved were less than 1%.

The shortest element length in the vicinity of the intersection was 4mm. However, it should be borne in mind that each 'p' element can recover stresses over a 10 by 10 internal grid an can have a shape function up to a 9^{th} order polynomial. The maximum deflection of 7.3mm occurred at the end of the horizontal leg as expected and this compared with an experimental value of 7.8mm. The deformations have been exaggerated in the scrap view in figure 4(a) to illustrate the ovalisation in the region of the intersection. Interestingly, the thin shell finite element results show that the maximum ovalisation does not occur at the intersection itself, but a small distance away (in this case 39.8mm). It should be noted however, that the maximum radial displacement is only 0.34mm and at the intersection it is only 0.28mm. It was not possible to measure such differences, using the experimental equipment available, to verify this finite element result.

4. Comparison of Results

4.1. Overall Deformations and Field Stresses

The end rotation of the horizontal leg, is compared with the value obtained from the finite element analysis in table 2. Also included in the table are the values derived for a beam representation of the mitre, in which there is no cross-sectional ovalisation. Reasonable agreement was obtained between experiment and finite element analysis, given the accuracy of the experimental measurement of rotation. The experimental results show slightly greater flexibility. This may be due to the fact that the fully fixed assumption used in the finite element model is not entirely realistic. However, it must also be noted that an 0.05 degree difference in an end rotation of 0.3 degrees is also on the limits of accuracy for the equipment used to measure rotation.

The results obtained from the 'membrane' check gauges on the vertical leg also compared reasonably well with the values from beam bending theory and finite element analysis. The thickness survey carried out on the bend showed a -3.4% variation in thickness in the region of the intrados, with only a -1.2% variation at the extrados. Stresses in the region of the check gauges are mainly membrane and will therefore vary inversely with thickness. This thickness variation does not entirely explain the difference between the experimental and finite element results however. Another contribution to the difference in results, is due to the fact that in the finite element analysis, the load was applied normal to the 'horizontal' leg, which in fact was not quite horizontal, due to the bend angle of 89.2 degrees. This small angle makes a difference of approximately $0.5N/mm^2$ at the check gauge positions, compared to a vertical load, due to the resulting variation in bending moment. Any lack of perpendicularity in the test rig set-up, of a similar magnitude, could also have resulted in similar variations. A slight lack of symmetry was also evident in the experimental results, from the check gauges, which is perhaps indicative of a lack of precision in the test geometry.

4.2. Stresses at Intersection

The maximum finite element stresses occur at the intersection and these values are presented in table 3.

The stress direction shown in table 3, is relative to the mitre intersection. The stress divisor used in calculating the Stress Concentration Factor was the nominal bending stress in a straight pipe of the same dimensions and with a moment M = F x Leg length i.e. $\frac{M}{\pi . r_m^2 . t}$.

For an in-plane moment tending to close the bend, the largest stress is compressive. As show in table 3, two almost identical values occur at different locations – one on the outer surface at 51 degrees and the other on the inner surface at 75 degrees. The former is in a direction normal to the intersection and the latter, along the intersection. For a load of the same magnitude opening the bend, all values of deflection, rotation and stress would have the same magnitude, but different signs (for small displacement linear elastic analysis).

Although not shown herein, it was observed that the directions of the principal stresses were perpendicular and parallel to the intersection (as expected from symmetry). The longitudinal distributions (experimental and FEA) show the angle of the principal stresses returning to the axial and circumferential directions, with increase in distance from the intersection. It was also apparent that the unsymmetrical nature of the transverse load was insignificant in regions close to the mitre, also as expected. The applied bending moment is obviously the same for each leg at the mitre intersection. This symmetry is confirmed by the fringe pattern shown in figure 4(b).

While the finite element results are obviously symmetrical about the 0º/180º positions, due to the applied constraints, the experimental results from the check gauges showed some slight lack of symmetry. This lack of symmetry became more evident at higher load levels and proved difficult to control by adjusting the loading ram. However, this

slight lack of symmetry is not sufficient to invalidate comparisons with FEA as illustrated by the following comparisons.

In figures 5 and 6, the outer surface principal stress distributions at 4mm from the intersection show good agreement in both form and magnitude. The inner surface experimental stresses also show reasonable agreement with the finite element analysis, in spite of the somewhat larger gauge sizes used on the inner surface. Preparation on the inner surface, for the purposes of gauge installation, was also affected slightly due to small surface imperfections very close to the intersection. Clearly the significance of any surface imperfections increases with the use of small gauge lengths.

The agreement for principal stress decay, shown in figures 7 and 8, is reasonable with the trends in distribution comparing particularly favorably. The comparison at the 60 degree location is better. The magnitudes of the stresses at this location are greater and the decay length is shorter. It is a common observation that experimental decay curves appear displaced from thin shell finite element distributions when modeling this type of intersection **[1]**. However, such 'displacement' is normally of the order of half a shell thickness at most. In the case of the mitre, the theoretical shell displacement 'δ' will vary depending whether the inside(+) or outside(-) surface is being considered, according to the relationship $\pm\left(\frac{t}{2}\tan\left(\frac{\psi}{2}\right)\right)\cos\theta$, where t is the shell thickness, 'ψ' is the mitre angle and 'θ' is the angular location, shown in figures 1 and 4. Clearly such a 'displacement' of distributions does not explain the differences between experiment and finite element analysis, in this case. The survey of wall thickness shows that the values at the 90 degree position in the vicinity of the mitre are 4.4% above average. A check on the proportions of bending and membrane stress at the 90 degree position, approximately 54mm away from the mitre intersection (where the differences are largest in figure 7), showed that the ratios are 2.5 and 8.4 for the two principal stresses. Given that the bending stresses which therefore dominate in this region, vary inversely with thickness squared, it is apparent that this thickness increase would result in a proportionately larger reduction in stress magnitude. This in itself would not explain the larger differences in figure 7. However, it is also possible that the thickening in the pipe wall at this location could lead to a reduction in ovalisation, which would in turn reduce the magnitude of the experimental results further. The fact that the thin shell finite element results are higher than the experimental values in general, is obviously conservative from a design viewpoint. In the case of the extrapolated 'hot-spot' stresses, the thin-shell over-estimate is of the order of 7 – 12%, as shown in table 4.

4.3. 'Hot-Spot' Stresses

Although the finite element extrapolation guidance in reference **[3]** is not intended for use with the highly refined mesh used for the mitre, it is informative to compare any differences arising from the various methods, when applied to a converged finite element model. Extrapolated hot-spot stresses obtained from the finite element and experimental results are compared with the 'raw' finite element results at the intersection in table 4. Both linear (2-point) and quadratic (3-point) extrapolation is used.

For extrapolation purposes, reference **[14]** recommends a strain gauge length of less than 0.2t (1.27mm in this case). As indicated in table 1, all gauges used for the mitre in the vicinity of the intersection satisfy this requirement. However, despite the 120 degree rosettes having an individual gauge length of only 0.38mm, the distance from the intersection to the centre of the closest rosette was 4mm, rather than the recommended 0.4t (2.54mm in this case). In the present investigation therefore, quadratic extrapolation was used for the experimental results, as values were available at 4/8/13mm, which is almost identical to the 4/8/12mm recommendations of reference **[3]**.

The values in table 4 appear encouraging. However, when the logarithmic nature of typical S-N curves is considered **[4]**, along with the slope of the curve, then such variations between finite elements and experiment may still result in significant differences in life predictions. It is not perhaps surprising that both linear and quadratic extrapolation provide similar results to the actual intersection stresses, given that the mesh is highly refined and converged to within 1%. However, the reversal in stress close to the mitre, as shown in figure 7, is not untypical for refined shell finite element models of intersection problems in general and clearly care would be required in such circumstances, with linear extrapolation in particular, to ensure that the correct trend is picked up. Bearing in mind that the present experiment used rosettes with individual gauge lengths of approximately a third of a millimetre, it would not have been possible to use more gauges, in an attempt to refine the experimental distributions. Not surprisingly, quadratic extrapolation provides more accurate results in this case. As expected, the thin shell results at the intersection represent a conservative position when compared with experiment. However, given the form of the decay distributions shown in figures 7 and 8, it is apparent that some stresses at the intersection may in fact be smaller when compared with results at the weld toe location. Given that the fatigue assessment procedures in some Codes **[4, 5]** requires stresses to be used in particular directions, which may not be the absolute maximum, it is important that both weld toe and intersection locations are considered.

The thin shell results at the intersection are very close to those obtained by extrapolation of the finite element results to the intersection. This is to be expected, given the highly refined nature of the mesh

The thin shell finite element results are in fact consistent in nature with through thickness linearization techniques illustrated in figure 2 for the weld toe position. Through thickness linearization techniques are used with 3-D solid models (and 2-D solid of revolution) to remove the peak stress component. Through-thickness linearization is an effective alternative to surface extrapolation methods and has the advantage of simplicity and is consistent with the use of linearization for other purposes in the Code design and assessment of vessels. It also has the advantage of being insensitive to the ‘stress reversal’ trends mentioned previously. The use of thin shell elements obviously means that such linearization is not required. Dong **[15]** has long been a proponent of a through-thickness linearization approach.

5. Conclusions

It is likely that better comparisons between experiment and finite element analysis could have been obtained by use of a more accurate test specimen with tighter tolerances on dimensions and manufacture. The use of 3D solid elements would also have served to eliminate the approximations inherent in shell solutions. However, this relatively 'simple' fabricated steel structure has highlighted many of the challenges faced in conducting effective experimental investigations and finite element studies involving welded discontinuous intersections of shells. Even with extensively instrumented specimens, using some of the smallest gauge lengths available, it is not always possible to pick up the local stress variations apparent in thin shell finite element models. For example, the experimental results do not exhibit the localized stress reversal shown in figure 7.

Such areas are susceptible to fatigue failure and the recovery of 'hot-spot' stresses is invariably dependent on accurate stress fields in the vicinity of the intersection. In this respect, the 'raw' finite element and experimental values for maximum stress at the intersection are in reasonable agreement. In addition, for the highly refined mesh used, there is little difference between linear and quadratic extrapolation techniques. All extrapolation techniques, when used with the finite element results, produce almost identical results to the 'raw' thin shell finite element values at the intersection. The extrapolated experimental 'hot-spot' stress values are however 7-12% lower than the 'raw' finite element results at the intersection. This level of variation should be borne in mind when assessing the accuracy of any fatigue analysis, as this can lead to significant variations in life prediction using the logarithmic S-N data.

The very local reversal in trend of the stress decay variation, which occurs in many shell intersection problems, can clearly cause errors with surface extrapolation techniques. It is worth noting that the through-thickness linearization approach to obtaining 'hot spot' or structural stress, using 3D solid elements, is not susceptible to this problem. These typical reversals in trend may also mean that the intersection stress value may not be the largest, as is often assumed. Some pressure vessel codes require stresses in particular directions to be used, which may be smaller in magnitude than the absolute maximum value of principal stress. These stresses, for cracks running in particular directions, may also have a lower allowable than the absolute maximum principal stress. It is important therefore that such trends in decay distributions are considered for thin shell models and that appropriate 'worst-case' scenarios are postulated. A finite element investigation using 3D solid elements could help to establish whether such a localized reversal in trend is a function of the thin shell idealization. Such a model would also be useful to study the location of the maximum position of ovalisation. A 3D solid representation would off course bring the additional problem of introducing a singularity.

Acknowledgements

The advice and assistance of my former colleagues David Cloney and George Findlay is gratefully acknowledged.

References

1. **Wood, J.** Observations on Shell Intersections; *4th World Congress on Finite Element Methods*; Interlaken; September 1984.

2. **Wood, J.** Procedural Benchmarks for Common Fabrication Details in Plate/Shell Structures; *NAFEMS Publication ISBN 1-874-376-02-6*; 2005.

3. **Niemi, E.** et al. Fatigue Analysis of Welded Components. Design Guide to the Structural Hot-spot Stress Approach (IIW-1430-00); *Woodhead Publishing Ltd.*; ISBN-13: 978-1-84569-124-0, 2006.

4. **B.S.I.** Specification for Unfired Fusion Welded Pressure Vessels; *PD5500*; 2000.

5. **B.S.I.** Eurocode 3: Design of Steel Structures; *BS EN 1993-1-9*; 2005.

6. **Peckover, R.S.** et al. *United Kingdom Offshore Steels Research Project – Phase 1 Final Report OTH 88 282*; UK Department of Energy; 1985.

7. **B.S.I.** Specification for Carbon Steel Pipes and Tubes with Specified Room Temperature Properties for Pressure Purposes; *BS3601*; 1987.

8. **B.S.I.** Tensile Testing of Metallic Materials: Method of Test at Ambient Temperature; *BS EN 10002-1*; 2001.

9. **Pople, J.** *BSSM Strain Measurement Reference Book*; British Society of Strain Measurement, 1979.

10. **Vishay.** Strain Gauge Installations with M-Bond 200 Adhesive; *Instruction Bulletin B-127*, Micro Measurement.

11. **Sobieszczanski, J.** Strength of a Pipe Mitred Bend; *J. of Engineering for Industry*, Nov. 1970.

12. **Edwards, G.** Cylindrical Shell Hybrid Finite Elements; *PhD Thesis*, University of Nottingham, 1974.

13. **Wood, J.** A Review of the Literature for the Structural Assessment of Mitred Bends; *Submitted for Publication to the Int. J. of Pressure Vessels and Piping*, Oct. 2006.

14. **Hobbacher, A.** Recommendations for Fatigue Design of Welded Joints and Components; *IIW Report XIII-1539-96;* Update June 2002.

15. **Dong, P.** A Structural Stress Definition and Numerical Implementation for Fatigue Analysis of Welded Joints; *Int. J. Fatigue, 23, pp865-876;* 2001.

LIST OF CAPTIONS

GAUGE NUMBER & ALIGNMENT	**GAUGE TYPE & INDIVIDUAL GAUGE LENGTH (mm)**	**INSTALLATION SURFACE & MANUFACTURER'S SPECIFICATION**	**DISTANCE FROM MITRE INTERSECTION TO CENTRE OF CONFIGURATION (mm) &** *ANGULAR POSITION (deg)*
1 to14; Normal to intersection	120º Rosette; 0.38mm	Outer; MM EA-06-015RC-120	**4**; *140,125-75 in 5 inc; 40, 10*
35 & 36; Normal to intersection	120º Rosette; 0.38mm	Outer; MM EA-06-015RC-120	**4**; *-90, -60* (Check gauges)
15 to 18; Middle gauge axial	120° Rosette; 0.38mm	Outer; MM EA-06-015RC-120	**8**, **13, 20.5, 28.5;** *90*
19 to 25; Middle gauge axial	90° Rosette; 1.37mm	Outer; MM EA-06-062RB-120	**42, 62.5, 84, 105, 126, 146.5, 457;** *90*
26 to 30; Middle gauge axial	120ºRosette; 0.38mm	Outer; MM EA-06-015RC-120	**8**, **13, 19, 25, 31;** *60*
31(1-5) Strip; Middle gauge axial	120° Rosette; 1.2mm	Outer; HBM 4/120 KY31	**37.5**, **41.5, 45.5, 49.5, 53.5;** *60*
32 to 34; Middle gauge axial	90° Rosette; 1.37mm	Outer; MM EA-06-062RB-120	**80, 146, 457;** *60*
37; Axial & hoop	90° Pair; 1.57mm	Outer; MM EA-06-062TT-120	**905**, *0*
38 & 40; Axial & hoop	90° Pair; 1.57mm	Outer; MM EA-06-062TT-120	**1000**, *90, -90*
39; Axial & hoop	90° Pair; 1.57mm	Outer; MM EA-06-062TT-120	**1095**, *180*
41 to 46; Middle gauge axial	90° Rosettes; 2mm	Inner; Showa N31-FA-2	**4**; *0, 45, 90, 0, -90, -45*

Note: Intrados = 0 degrees and Extrados = 180 degrees.

Table 1. Details of strain gauges.

	Rotation of Horizontal Leg (deg)	Vertical Deflection @ End of Horizontal Leg (mm)	Maximum Principal Stress @ Extrados 1000mm from mitre (N/mm^2)	Maximum Principal Stress @ Intrados 1000mm from mitre (N/mm^2)
Experiment	0.35	7.8	28.3	-32.7
Beam Theory (no ovalisation)	0.16	3.7	27.5	-29.8
FEA	0.30	7.3	28.4	-30.2

Table 2. Comparison of Overall ‘Deformation’ and Field Stresses.

	Maximum Principal Stress (N/mm^2)	Angular Position θ (deg)	Stress Direction	Maximum SCF	Minimum Principal Stress (N/mm^2)	Angular Position θ (deg)	Stress Direction	Maximum SCF
Outer Surface	151.7	84.0	Normal	5.2	-285.7	50.6	Normal	-9.8
Inner Surface	211.1	43.5	Normal	7.2	-285.8	74.5	Hoop	-9.8

Table 3. Maximum Finite Element Stresses at Intersection.

	FE Thin Shell @ Intersection (N/mm^2)	FE Thin Shell Extrapolated 0.4t/1.0t (N/mm^2) **[3]**	FE Thin Shell Extrapolated 4/8/12 mm (N/mm^2) **[3]**	Experimental Extrapolated 4/8/13 mm (N/mm^2)
Outer Surface @ 90 degrees	123.3	126.3	125.0	114.7
Inner Surface @ 90 degrees	-94.1	-95.9	-94.2	-
Outer Surface @ 60 degrees	-269.3	-263.5	-266.8	-239.2
Inner Surface @ 60 degrees	155.9	151.3	154.2	-

Table 4. Maximum Finite Element Stresses at Intersection.

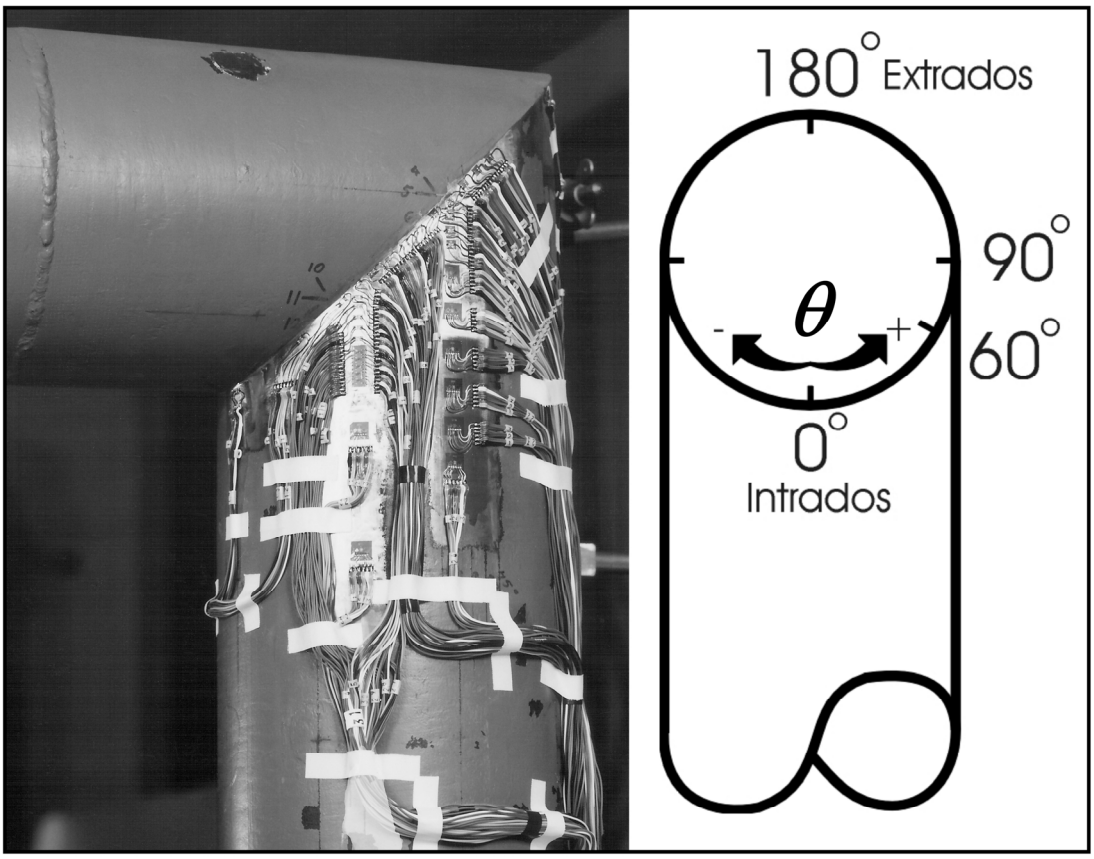

Figure 1. Mitred Bend Showing Strain Gauges.

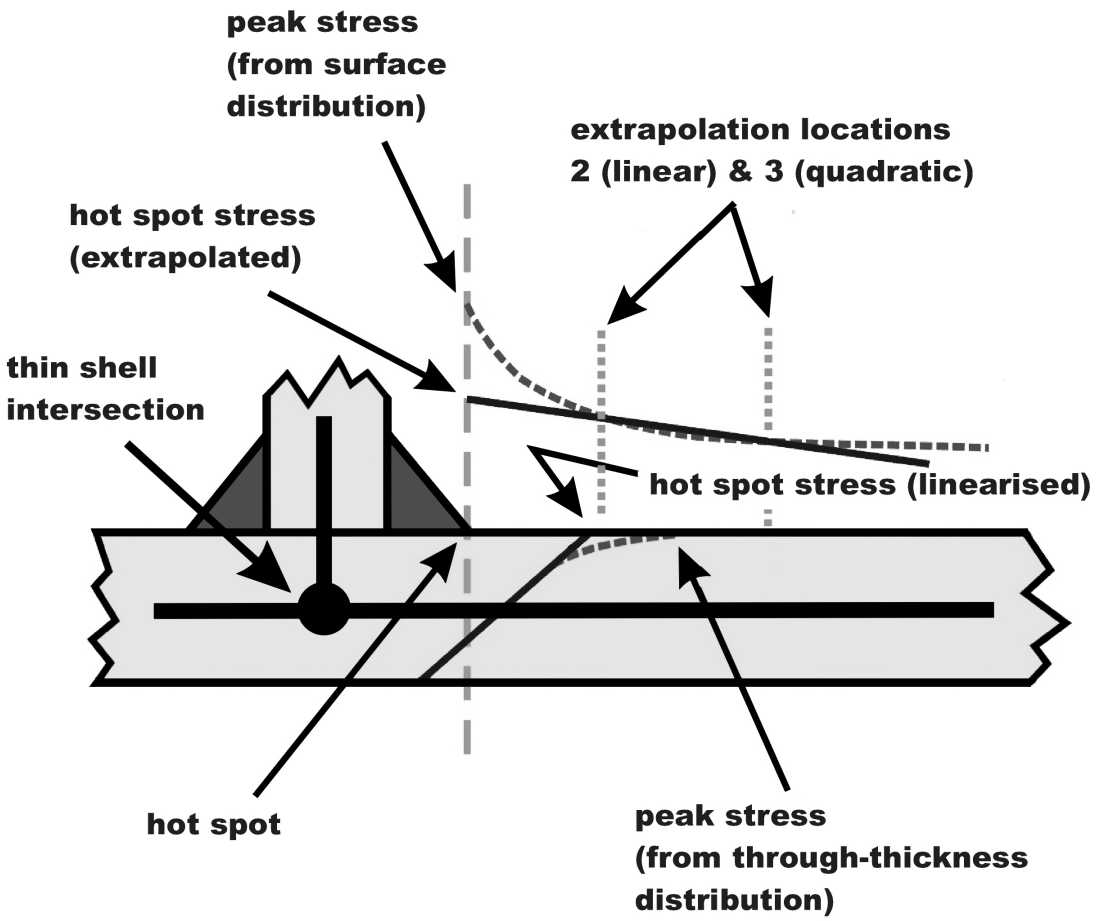

Figure 2. Various Hot Spot Stress Techniques for Intersections and Welds.

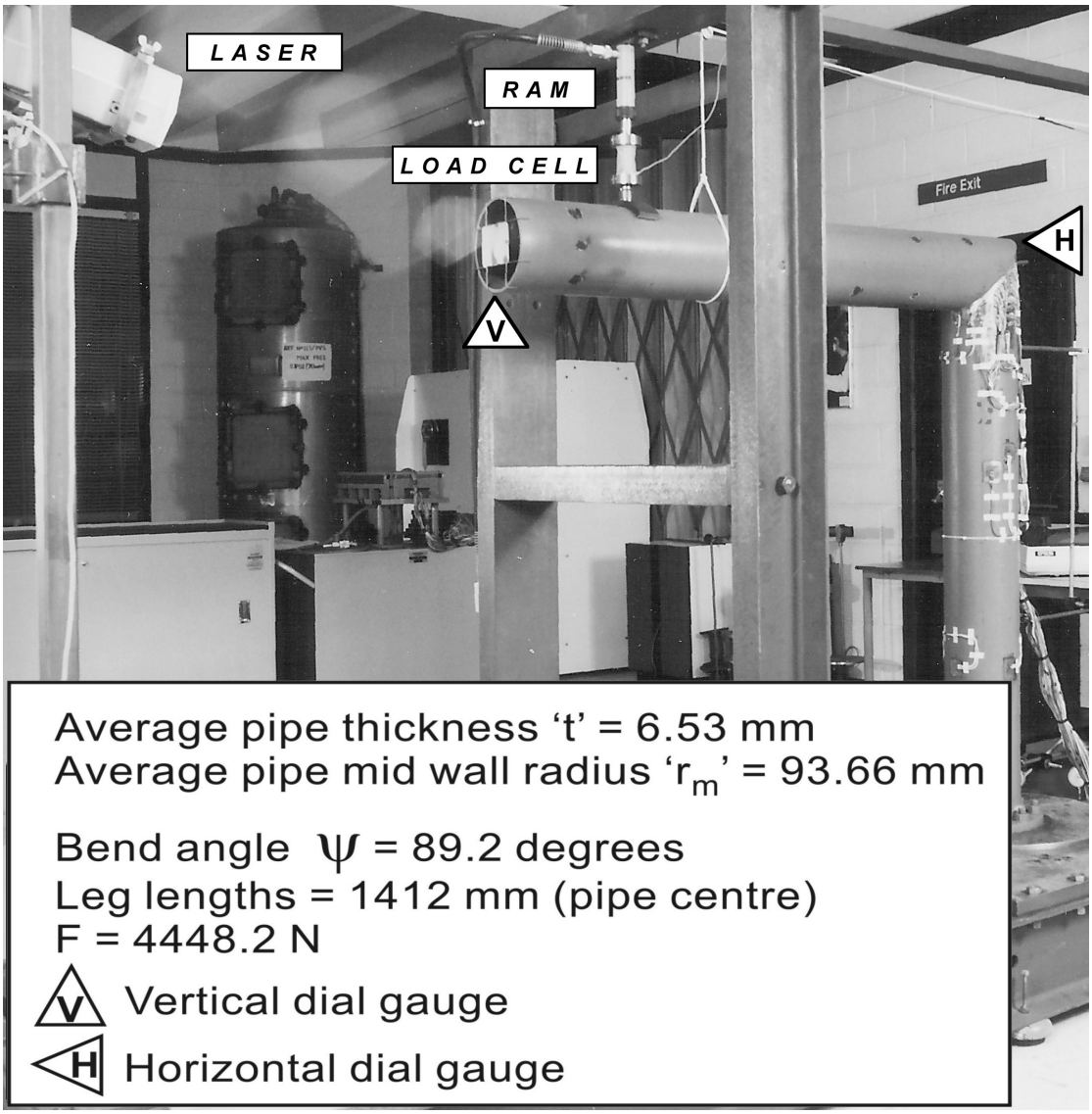

Figure 3. Test Arrangement for Mitred Bend.

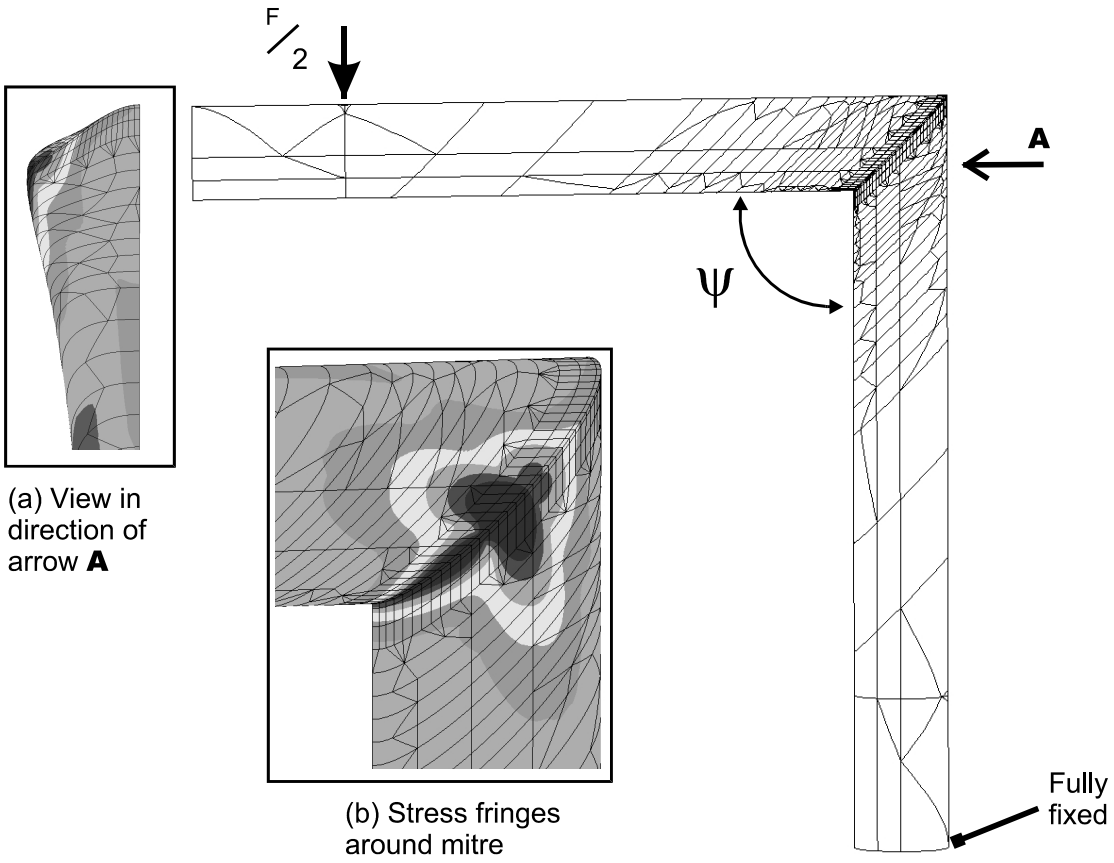

Figure 4. Adaptive P-method Finite Element Model with von Mises Stress Superimposed on Deformed Shape.

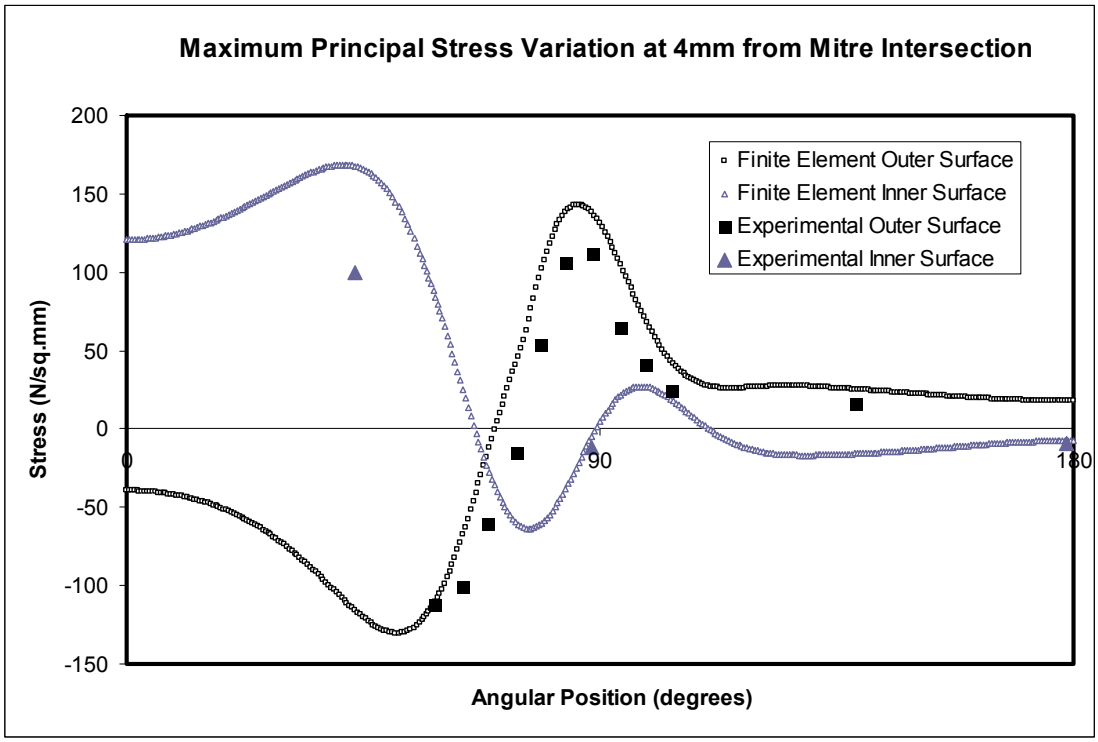

Figure 5. Maximum Principal Stress Variation Near Mitre Intersection.

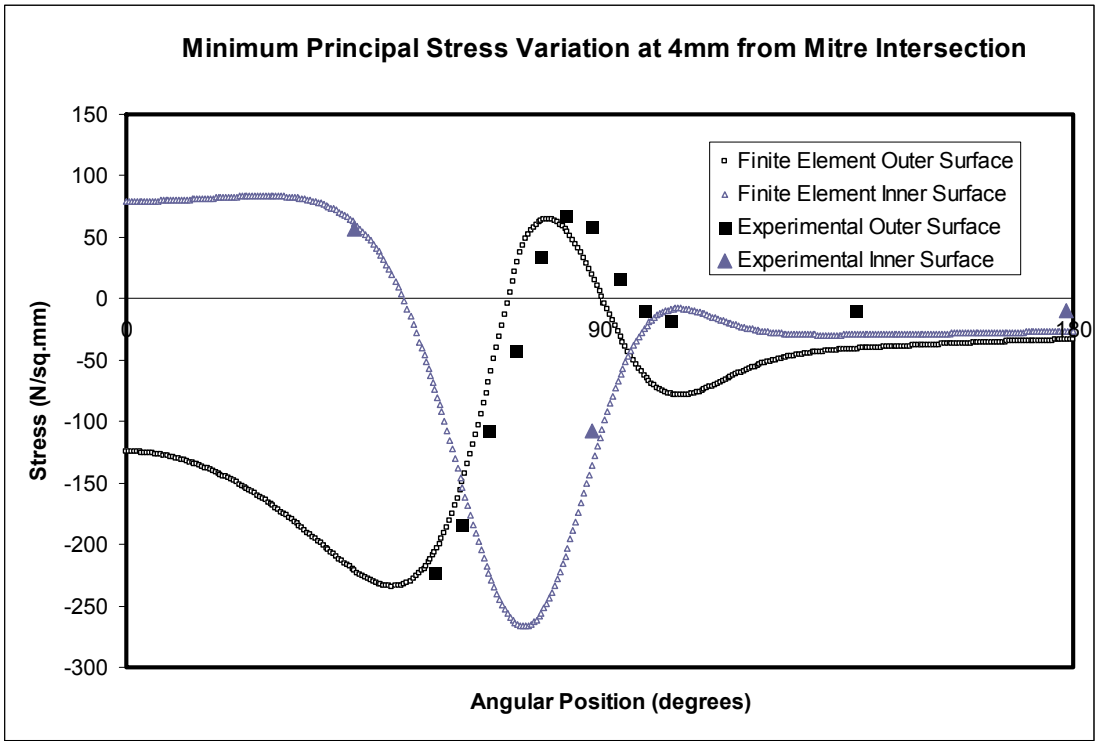

Figure 6. Minimum Principal Stress Variation Near Mitre Intersection.

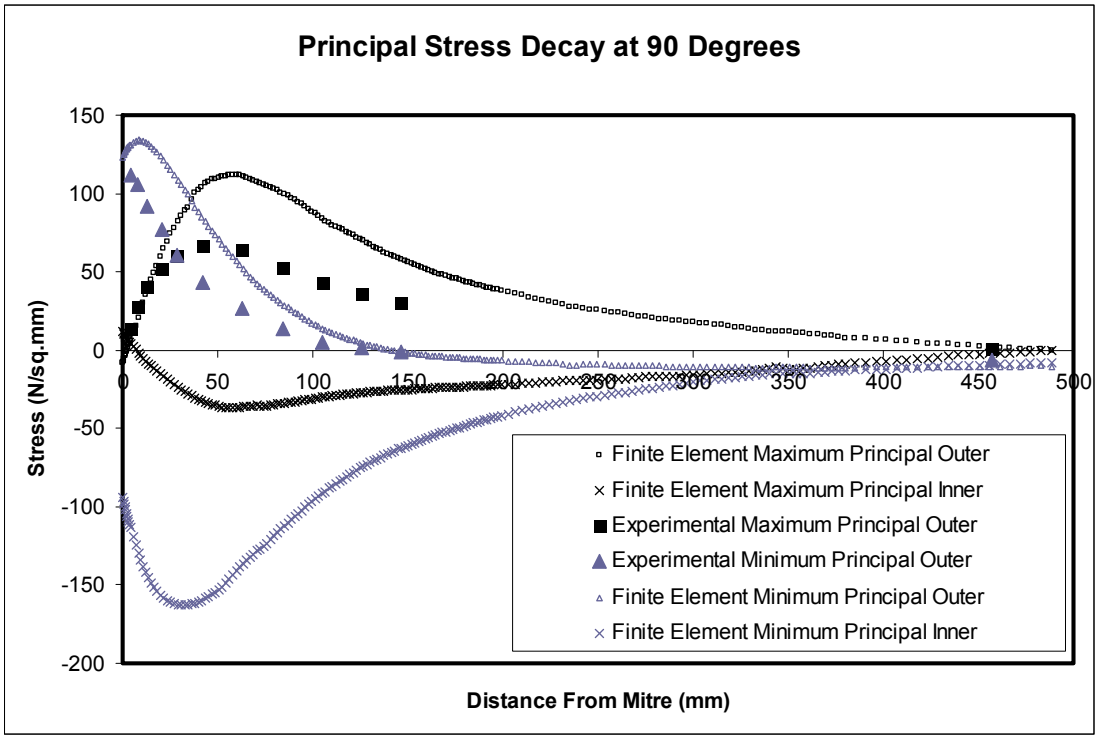

Figure 7. Principal Stress Decay at 90 Degree Location.

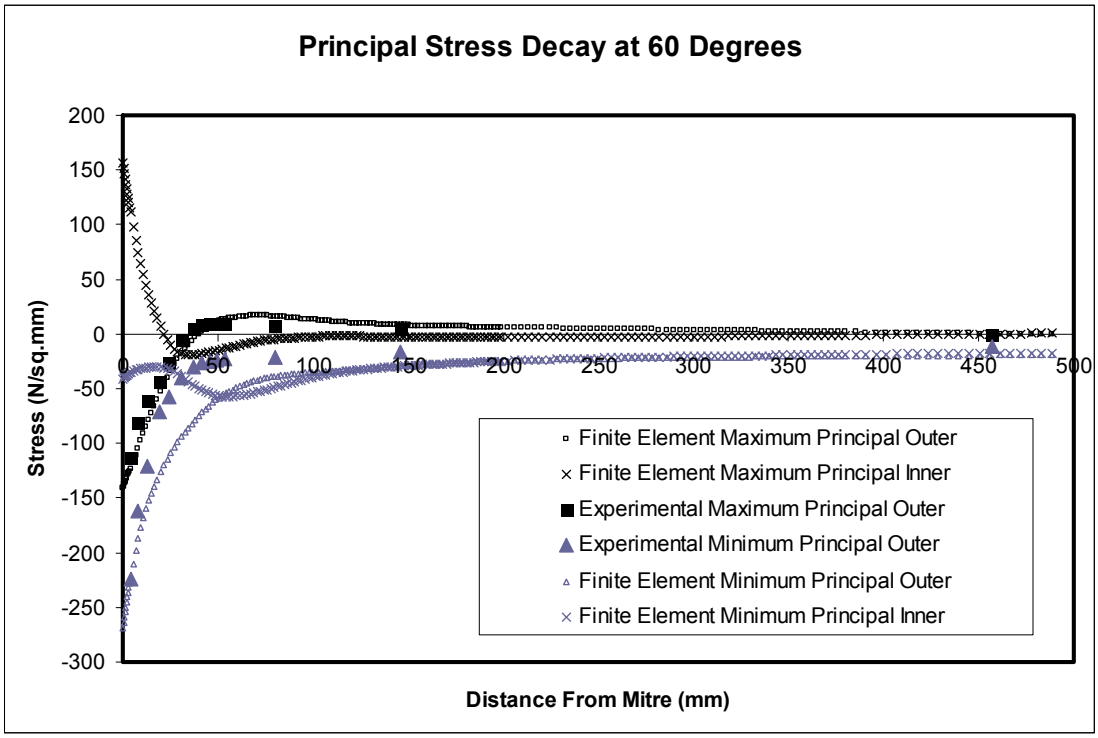

Figure 8. Principal Stress Decay at 60 Degree Location.